JOURNAL OF MATERIALS SCIENCE **35** (2000) 4937–4943

Experiments and analyses on tensile behaviour of a TiAl alloy with lamellar structure

MIN FU, YOUSHI HONG, YOULI MA
State Key Laboratory of Nonlinear Mechanics, Institute of Mechanics, Chinese Academy of Sciences, Beijing 100080, People's Republic of China
E-mail: Hongys@LNM.imech.ac.cn

SHIQIONG LI
Department of Superalloys, Central Iron and Steel Research Institute, Beijing 100081, People's Republic of China

An as-cast Ti-47Al-I Cr-2.5V plate was used to perform ambient tensile test. The metallography of the specimen exhibits typical lamellar structure with two-phase titanium aluminides. Monotonic tension tests under mechanical test systems of MTS-810 and Scanning Electron Microscope (SEM), along with a novel holder, were carried out regarding microstructure influence on crack initiation. Test results give the orientation preference of initiated cracks, i.e. 40°, 60° and 90°. Furthermore, with respect to crystallography and a model of interface mechanics, related mechanisms are discussed.

1. Introduction

Extensive research activities have been conducted on two-phase titanium aluminides for more than a decade due to their low density and high strength at elevated temperatures. However, its low elongation and toughness at room temperature, and difficulty for hot working seriously retard its engineering application. With comprehensive considerations, relevant work now comes to a stage of developing a kind of low cost and reliable TiAl [1].

Many studies revealed [1–3] that TiAl with fine full-lamellar structure can balance such mechanical properties as strength, elongation and toughness. However, the microstructure of TiAl fabricated by ordinary casting technique pertains to coarse lamellar grains. If fine full-lamellar structure could be obtained just with the way of alloying or any other improved technique in casting, it would markedly reduce the number of steps of processing, cut cost and directly turn out parts with complicated shape. And, it will benefit industries of aerospace, land and marine carrier in need of structural materials with low-weight and high-temperature resistance.

In fact, if loading orientation is selected properly, even single "grain" with full lamellar structure of the so-called "polysynthetically twinned (PST) crystals", may exhibit good strength and elongation at ambient temperature [2]. As revealed in some studies [4, 5], within lamellar structure there are three γ/γ intervariant lamellar boundaries, i.e. true-twin, pseudo-twin and domain types in addition to γ/α_2 lamellar boundary. The delamination of lamellar boundaries has been found to occur mostly among γ/γ interfaces at room temperature but along both γ/γ and γ/α_2 interfaces at high temperatures [2]. However, the mechanism of microstructure effect on fracture failure is not very clear yet. Thus, more investigations should be done to add the knowledge of effect of intervariant lamellae.

In this paper, for making clear relevant mechanism of TiAl lamella interaction, a kind of as-cast TiAl specimen with plate shape was used to study the behaviour of tension at room temperature. The work mainly focuses on the observation of the crack initiation, microstructure influence, and related analyses with crystallography and interface mechanics.

2. Experimental procedure

An original Ti-47Al-1Cr-2.5V plate was prepared with a cold crucible induction and melting technique by centrifugal casting, and followed by 4 hour hot isostatic pressing (HIP) at conditions of 1260°C, 172 MPa and argon medium. Test specimens were prepared by electric spark cutting from the as-cast TiAl plate, and polished to reach 0.06 μm of R_a by a grinding machine with diamond abrasive of 2.5 μm in diameter, where R_a is the average roughness of specimen surface. With consideration of limit room of SEM loading stage, the geometry of specimen for *in situ* tensile test is of small size. Those specimens are illustrated in Fig. 1 for monotonic tension under MTS-810 (a) and SEM testing system (b).

Polished surface of the as-cast TiAl plate shows its metallography of full lamellae (Fig. 2) after etching. The mean size of colonies is around 400 μm with the range of 100–800 μm in normal distribution so that we could easily get almost all colonies in size of about 0.4 mm within the gauge length of the cut specimens.

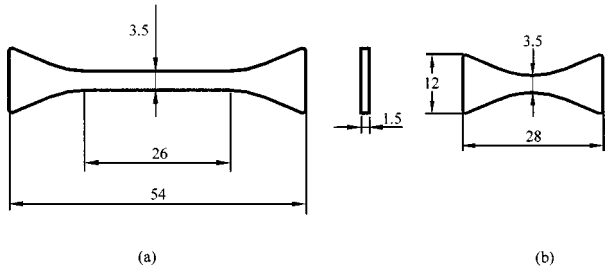

Figure 1 TiAl plate specimens for monotonic tension under (a) MTS-810 testing machine and (b) SEM loading system (dimensions in mm).

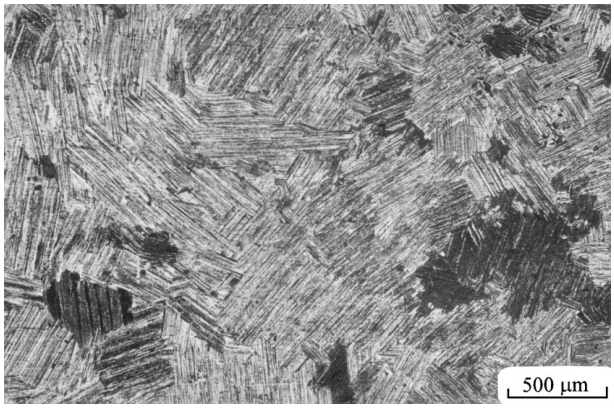

Figure 2 Microstructure of the as-cast TiAl in fully lamellar form.

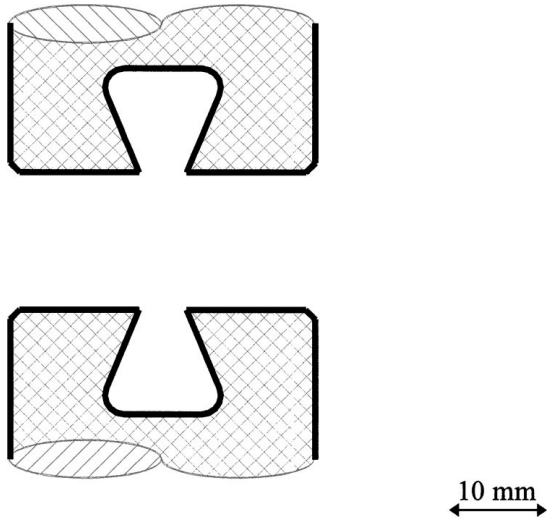

Figure 3 Special loading grippers for plate-shape specimen.

Relevant tests were carried out by adopting a novel holder with a special fixture [6], which can ensure good loading alignment and afford a way of non-screw connection between plate-type specimens and grippers (Fig. 3).

Tensile tests under MTS-810 testing system were carried out at a strain rate of 6.67×10^{-6} s^{-1} to measure the mechanical properties of elastic modulus, elongation, strain hardening exponent, yield strength and ultimate strength. Experiments were also performed under SEM tensile system at a gripper-moving velocity of around 1 μm/s so as to investigate the characteristics of crack initiation and propagation interacted with the microstructure. The upward surface of specimen is for the *in situ* observation and the downward surface of specimen was stuck with a strain gage for deformation measurement.

3. Experimental results

Fig. 4 shows the curve of nominal stress $\bar{\sigma}$ versus nominal strain $\bar{\varepsilon}$. The strain-hardening exponent (n) can be obtained from the plastic portion ($\varepsilon_f > \varepsilon_p > 0.002$) of the true stress [$\sigma = \bar{\sigma}(1+\bar{\varepsilon})$] - true strain [$\varepsilon = \ln(1+\bar{\varepsilon})$] curve according to the Hollomon equation ($\sigma = k\varepsilon_p^n$). Table I lists the corresponding result, which were obtained from the data of 3 specimens.

As shown in Fig. 4, there is no yielding instability, and no detectable necking phenomena within the gauge length of the specimen. The ultimate strain is only 0.0067, showing the brittle propensity of the as-cast TiAl alloy. The strain-hardening exponent of 0.12 is determined by using Hollomon equation with good correlation coefficient of 0.99, which is in the data range the conventional high strength steels possessed. But its yield strength (305 MPa), ultimate fracture strength (360 MPa) and elastic modulus (134 GPa) are comparatively low. Perhaps, such special tensile behaviour may be attributed to the microstructure and the geometry of plate-type. As indicated in the above text, the maximun colony size of the cast plate is about 0.8 mm, and the mean size is 0.4 mm. The specimens we used in the test contain 4–5 colonies in the thickness direction even though the whole thickness of specimens is merely 1.5 mm. The tensile results shown in Table I are similar from specimen to specimen and the fracture sites are located at the middle of the specimens.

As a next step of the investigation, *in situ* tests were performed under the tensile stage of SEM. Characteristics of crack initiation and propagation are observed. Those phenomena reflect effects of main microstructure features such as orientation of lamellar boundary, and grain size.

TABLE I Mechanical properties of tested as-cast TiAl

$\sigma_{0.2}$ (MPa)	E (MPa)	$\sigma_u \approx \sigma_f$ (MPa)	ε_f	n	R
305	1.34×10^5	360	0.0067	0.12	0.99

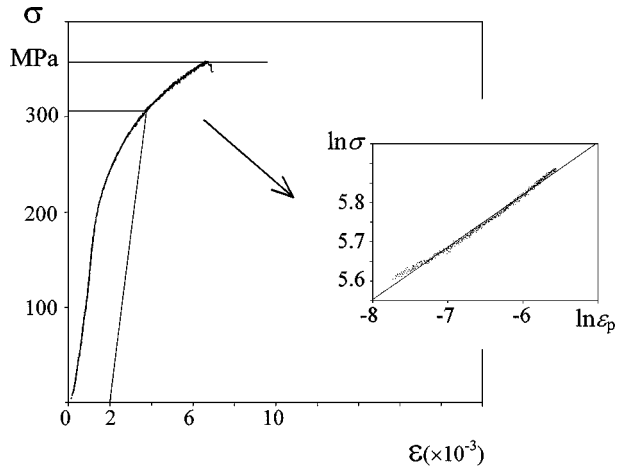

Figure 4 Stress vs. strain curve of TiAl specimen, and its fit curve with Hollomon equation ($\sigma = k\varepsilon_p^n$).

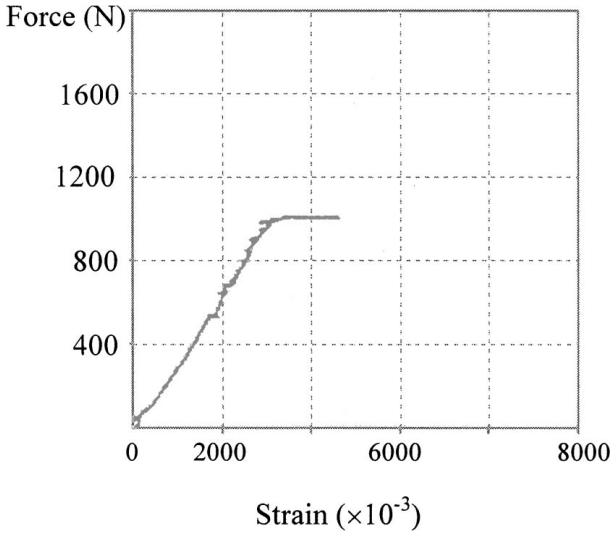

Figure 5 Load-strain curve of plate-type TiAl specimen, test terminated upon crack initiating under *in situ* tension of SEM. Noting that there is a load-increasing stop with a jump in strain value in the end of the curve.

With respect to crack initiation, there are three noticeable features, i.e. sudden crack initiating, site preference and orientation preference. Fig. 5 is a load-strain curve terminated upon crack initiating. The load stopped increasing with a jump in strain value to form a plateau at the ultimate load (Fig. 5). Meanwhile, one to three cracks can be observed in a specimen under SEM, as shown in Fig. 6. Another phenomenon is site preference, which is also shown in Figs 6 and 7. Initiated cracks are mainly due to delamination within grains. Apart from this, a kind of "short" cracks can also initiate at the boundary of grains. Such "short" cracks, whose size is comparable with the thickness of layers, all run nearly perpendicular to their local lamellar boundary (Fig. 7), whereas those interlamellar cracks, whose size is comparable with the dimension of their local grain, run parallel to their lamellar boundaries (Fig. 6). The latter plays more important role in the final fracture. While short cracks at grain boundaries of can only contribute a damage in specimen due to tension. The third impressive phenomenon of crack initiation is the crack orientation preference. As indicated in Fig. 8, there are several peaks of crack orientation angle. The orientation defined in this paper is the angle (ψ) between crack plane to the loading axis. Thus, from our measurements, angles of 40, 60 and 90 degrees are the inclinations of most initiated cracks. Related mechanism is discussed later in this paper.

During crack propagating, there are also three obvious characteristics, i.e. rapid propagating, translamellar fracture and deflecting of propagating cracks. Fig. 9 shows that a crack is propagating in translamellar mode. For the deflection of cracks, that phenomenon happens at either inner or boundary of grains. Fig. 10a exhibits a typical deflection (within the white circle) caused by crack-ligament shearing. There are two types of boundary deflection. As shown in Fig. 10b, if interlamellar crack encounters a grain with large difference in orientation, the crack will deflect along their boundary. If the orientation of the encountered grain is close to that of interlamellar crack, the crack will deflect to delaminate the neighbour grain (Fig. 10c).

4. Discussion

There are two interesting phenomena worthy of discussion. One is that an initiated crack runs along lamellar boundary within grains, and another is its orientation preference (Fig. 8). Here, a question can thus be brought out, that is what is responsible for both phenomena. In general, there are no other than two causes that can account for the experimental phenomena, i.e. binding strength and deformation mismatch of intervariant lamellae. Both are coherent with structures of lamellae.

As to the structures of lamellae, there are two kinds of phases, i.e. γ-TiAl (ordered tetragonal structure $L1_0$) in majority and α_2-Ti_3Al (ordered hexagonal structure $D0_{19}$) in minority. For full lamellar TiAl alloy, in addition to α_2/γ, there are six orientations of γ that are illustrated in Fig. 11 for their habit plane. As shown in this figure, apart from the atom arrangement in the habit plane of α_2-Ti_3Al, all six possible ones of γ-TiAl are arrayed in a table. The six orientations of γ are designated as γ_1^{I}, γ_2^{II}, γ_3^{I}, γ_4^{II}, γ_5^{I} and γ_6^{II} in order of a 60°-rotation-angle increment. Here, "I" and "II" mean different stacking sequences, i.e. "ABCABC……" and "CBACBA……". Thus, we can represent domain, twin and pseudo-twin relationships of variant γ lamellae with $\gamma_1^{\mathrm{I}}/\gamma_n^{\mathrm{I}}$ ($n=3, 5$), $\gamma_1^{\mathrm{I}}/\gamma_4^{\mathrm{II}}$ and $\gamma_1^{\mathrm{I}}/\gamma_n^{\mathrm{II}}$ ($n=2, 6$)

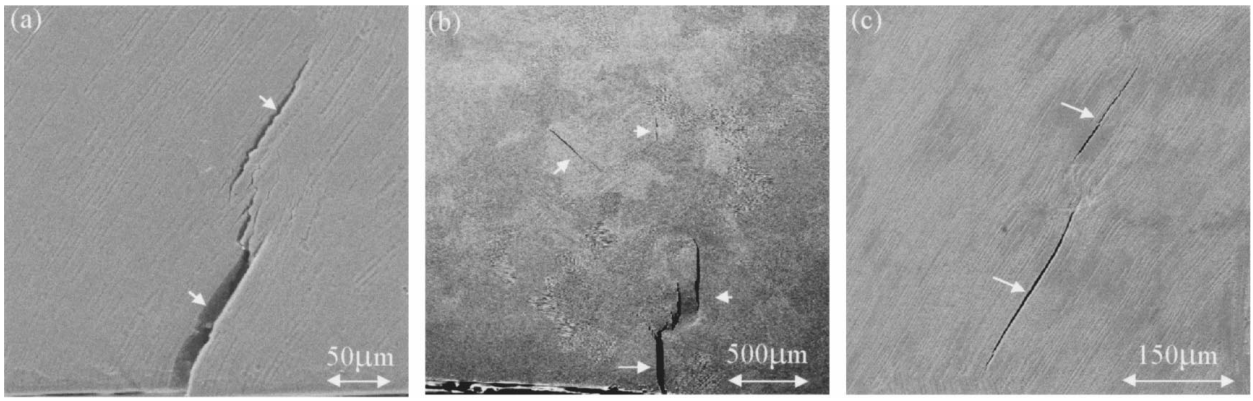

Figure 6 Initiated cracks (indicated by white arrow) within specimens of the TiAl specimen under tensile stage of SEM at tensile velocity of 1 μm/s. (a) at strain of 0.3%, (b) at strain of 0.4%, (c) at strain of 0.45%. (Loading direction is horizontal).

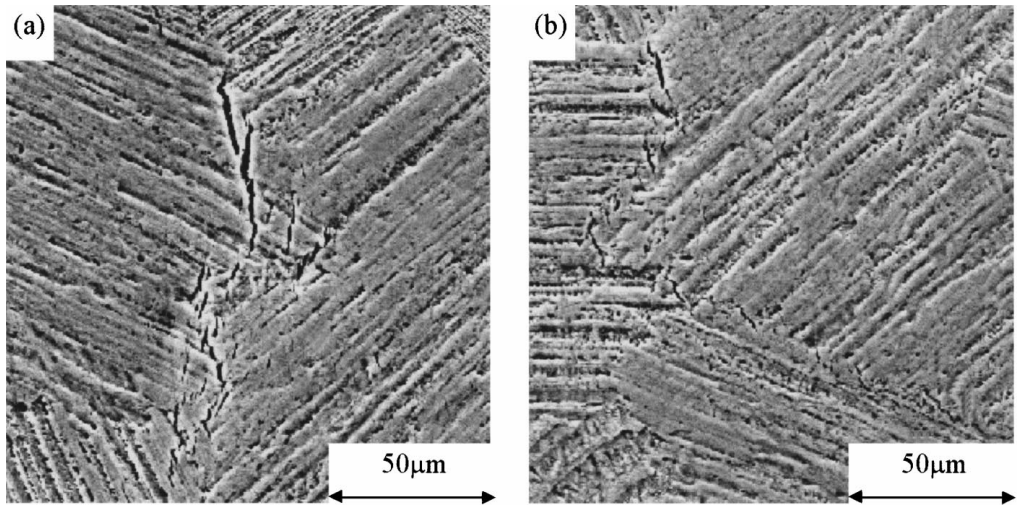

Figure 7 Short cracks at grain boundaries of the TiAl specimens under *in situ* testing sysytem of SEM at strain of 0.4%. (Loading direction is horizontal).

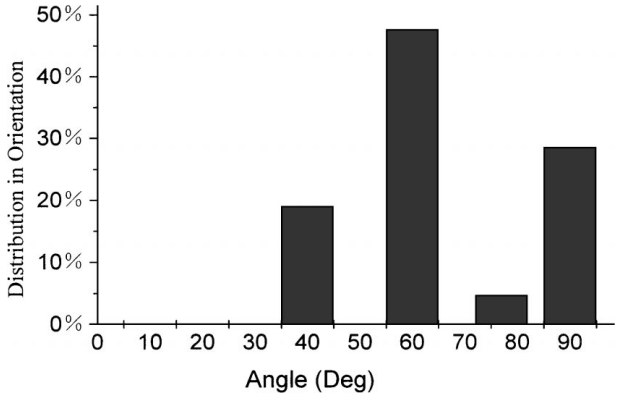

Figure 8 Orientation preference of initiated cracks of TiAl specimens with fully lamellar structure, showing three inclinations, i.e. 40°, 60° and 90° (ψ).

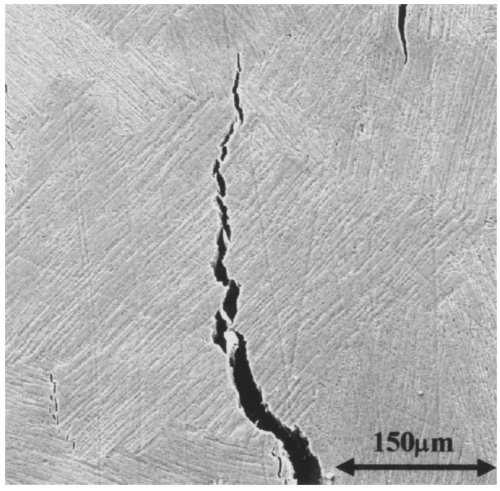

Figure 9 Propagating crack in translamellar mode within TiAl specimen under *in situ* testing system of SEM at tensile velosity of 1 μm/s (test terminated at strain of 0.53%). (Loading direction is horizontal).

respectively. In addition to γ/α_2 interface, there exist five rotational relationships of γ interlamellae. In each lamella there are only γ domains.

Due to the variant orientations of lamellae, atom misfit exists at the boundary of two neighbor lamellae. If the basal plane of γ_1^{I} is combined with that of γ_2^{II}, or γ_3^{I}, or γ_4^{II}, or γ_5^{I}, or γ_6^{II}, or α_2 together, the number of Al-Ti (NAT) can be taken into an account of atom mis-fit. Thereby, we can obtain that there is zero (0, perfect fit) of NAT in $\gamma_1^{\mathrm{I}}/\gamma_4^{\mathrm{II}}$ of twin relationship, six (6, medium fit) of NAT in $\gamma_1^{\mathrm{I}}/\gamma_2^{\mathrm{II}}$, γ_3^{I}, γ_5^{I}, γ_6^{II} of domain and pseudo-twin relationships, and nine (9, low fit) of NAT in α_2/γ relationship.

In fact, NAT should play an important role in binding strength of neighbor lamellae. Based on the above structural relationship, the boundary of α_2/γ should have the highest binding strength, whereas that of twin relationship has the lowest one. In other words, the boundary with large value of NAT should have high resistance to crack initiation at room temperature. Crack propagating can almost reflect interface-binding strength. Thus, we can compare the presumption with relevant experiments. As indicated in the tests of Ref. [7], the relative ease of crack propagating along adjacent lamellae is given by: $\gamma_1^{\mathrm{I}}/\gamma_4^{\mathrm{II}}$ (twin related) $>\gamma_1^{\mathrm{I}}/\gamma_2^{\mathrm{II}}$, γ_3^{I}, γ_5^{I}, γ_6^{II} (domain and pseudo-twin related) $>\alpha_2/\gamma$, which is consistent with the tendency of our NAT analysis.

The compatibility of deformation may play more important role at the stage of crack initiation. Here, we introduce a geometric compatibility factor ($\tilde{m}$) [8] to define the extent of deformation compatibility for adjacent lamellae. The geometric compatibility factor, $\tilde{m}$, can be calculated as

$$\tilde{m} = \cos\varphi \cos\lambda \tag{1}$$

where φ is the angle between the normal to the slip planes of adjacent lamellae, λ the angle between the slip directions of them.

Owing to the f.c.c structure of γ lamellae, we may use Thompson tetrahedron to represent all slip systems of a lamella. As indicated in Ref. [9], there are three major deformation mechanisms, i.e. twinning, ordinary slip and superlattice slip, and, there is little difference in critical dissolved shear stress (CRSS) among them at room temperature. So, it allows for analyzing compatibility of deformation just with $\{111\}<110]$ slip

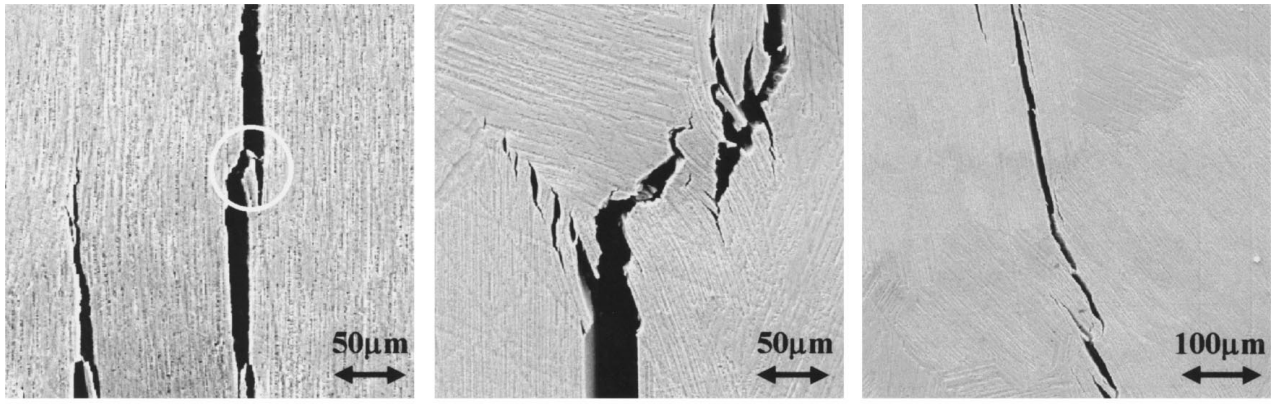

Figure 10 Crack deflecting (a) within a grain (circled zone), (b) along grain boundary and (c) along lamellar interface of neighbour grain of TiAl specimen with fully lamellar structure (terminated at strain of 0.5%). (Loading direction is horizontal).

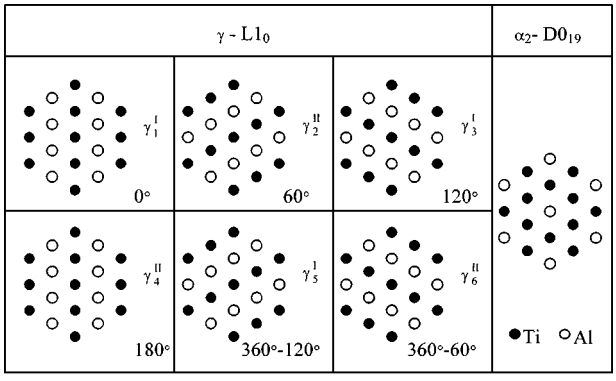

Figure 11 Six orientations of the habit plane of the γ phase with respect to the basal plane of the α_2 phase. "I" and "II" represent respective stacking sequences, i.e. "ABCABC…" and "CBACBA…"; Relevant angles all take γ_1^{I} as a reference.

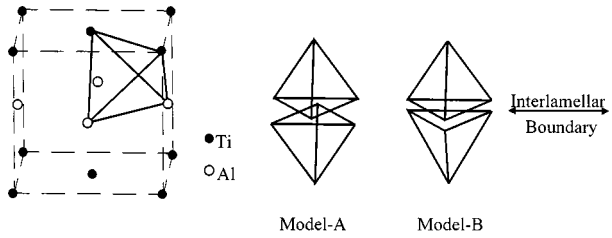

Figure 12 Two resembling models in Thompson tetrahedron for variant γ-interlamellae. $\gamma_1^{\mathrm{I}}/\gamma_1^{\mathrm{I}}$, $\gamma_3^{\mathrm{I}}/\gamma_1^{\mathrm{I}}$, $\gamma_5^{\mathrm{I}}/\gamma_1^{\mathrm{I}}$ belong to the model A, $\gamma_2^{\mathrm{II}}/\gamma_1^{\mathrm{I}}$, $\gamma_4^{\mathrm{II}}/\gamma_1^{\mathrm{I}}$, $\gamma_6^{\mathrm{II}}/\gamma_1^{\mathrm{I}}$ come under the model B.

systems (ordinary and superlattice slip related) even though there is also a kind of twinning-slip system of $\{111\}<11\bar{2}]$.

Regarding the relationships of intervariant γ lamellae (shown in Fig. 11), we get two different kinds of orientation relationship between tetrahedrons of adjacent γ lamellae, as illustrated in Fig. 12. If we take γ_1^{I} as a fixed reference layer, orientation relationships of tetrahedrons for $\gamma_3^{\mathrm{I}}/\gamma_1^{\mathrm{I}}$ and $\gamma_5^{\mathrm{I}}/\gamma_1^{\mathrm{I}}$ can be related to the model A (Fig. 12), $\gamma_2^{\mathrm{II}}/\gamma_1^{\mathrm{I}}$, $\gamma_4^{\mathrm{II}}/\gamma_1^{\mathrm{I}}$ and $\gamma_6^{\mathrm{II}}/\gamma_1^{\mathrm{I}}$ to the model B (Fig. 12). Further, comparing the maximum of $\tilde{m}$ of all possible slip systems except for those which parallel to their interlamellar boundary, we can readily obtain that, $\tilde{m}$ in the model A is 1, whereas in the model B, it is only 0.648 ($\cos\phi = 7/9$, $\cos\lambda = 5/6$). Obviously, 120°-rotation relationship (domain related) of γ lamellae has better compatibility of deformation, which has been proved by some studies [4, 8], whereas, 60° (pseudo-twin related) and 180° (twin related) have lower compatibility of deformation.

Due to low NAT and geometric compatibility factor in twin relationship, we can deduce theoretically that adjacent lamellae of twins are prone to delaminating during either crack initiation or crack propagation. In fact, α_2 phase has a smaller number of slip systems. Thus, γ/α_2 should have the lowest compatibility of deformation. But, regarding its high NAT, the influence of such interface or crack initiation is not clear.

Another analysis of a crack between dissimilar media has been given by several authors, e.g. Dundurs [10], Hutchinson *et al.* [11], Rice [12], Shih *et al.* [13], etc. The two Dundurs' parameters [10], designated as α and β, are still extensively used in analyzing crack-tip fields at the interfaces of isotropic linear elastic media [14]. Base on their work, the crack-tip fields for the case of linear isotropic media take the form [13]

$$\sigma_{ij} = \sum_{n=1}^{2} \frac{Q_n}{\sqrt{2\pi r}} g_{ij}^{(n)}[\theta, \varepsilon, r, a] \tag{2}$$

where Q_n is the complex stress-intensity factor, $g_{ij}^{(n)}[\theta, \varepsilon, r, a]$ is a function that varies in form with i and j of the polar indices (r, θ) [13], a the semi-length of a crack, and ε the "oscillation index" given by

$$\varepsilon = \frac{1}{2\pi} \ln\left(\frac{1-\beta}{1+\beta}\right) \tag{3}$$

which is regarded as the extent of elastic mismatch. Now, as to our lamellar structure of TiAl, suppose that there is a presumed crack at a lamellar boundary, which is based on the presumption of the same failure criterion in toughness for pre-cracked and non-pre-cracked specimens, the presumed semi-length of a crack, a, may then be expressed as

$$a = \frac{K_{\mathrm{Ic}}^2}{\pi \sigma_{\mathrm{b}}^2} \tag{4}$$

where K_{Ic} is mode I fracture toughness, and σ_{b} the monotonic tensile strength. Regarding orientations

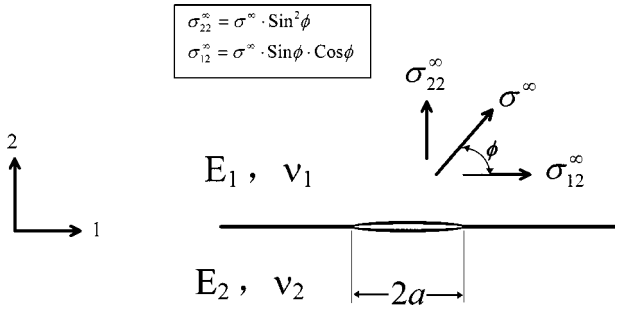

Figure 13 Loading model for dissimilar materials. a is the semi-length of cracks; and E_i and ν_i indicate Young's modulus and Poison ratio repectively, of two materials; ϕ is the angle between directions of remote loading stress (σ^{∞}) and the interface of dissimilar materials.

of lamella boundary or remote loading, the loading model can be illustrated in Fig. 13 in which "ϕ" is the angle between directions of loading and interface.

In terms of the above, we can calculate the stress field in front of presumed crack tip to obtain the influence of the ϕ and ε. According to the result illustrated in Fig. 14, with the growing of ε, the angle of ϕ for the maximum of shear stress (σ_{12}) goes from 45° ($\varepsilon = 0$) to smaller angles, e.g. 38° ($\varepsilon = 0.2$), while, that of the maximum of normal stress (σ_{22}) moves from 90° at $\varepsilon = 0$ to 83° at $\varepsilon = 0.2$.

The above model can semiquantitatively give an explanation for our experimental result about orientation peaks (ψ) of nucleated cracks, i.e. 40°, 60°, 90°. Obviously, cracking at 90° is associated with the normal stress (σ_{22}), and, cracking at 40° should be more relevant to the shear stress (σ_{12}). While, cracking at 60°, the highest peak, may be associated with a synergic impact from both σ_{12} and σ_{22}. Note that the orientations are determined at two-dimensional space, they could have a little difference with those at three-dimensional space.

With a view to the deformation anisotropy and mismatch due to the aforementioned crystal structures of γ and α_2 lamellae, the value of ε may be greater than the one obtained by Equation 3. Thus, the way for correcting the value of ε is worth studying. Even though stiffness matrix can theoretically give a way to cope with the problem, there are complexity and difficulty in obtaining relevant parameters. In view of all above, comparatively simple and integrated expression of failure criterion in regard to σ_{12}, σ_{22}, ε, NAT and $\tilde{m}$ should be established to propose the related mechanism of cracking along interfaces between intervariant lamellae, which awaits further experimental work and theoretical analysis in the coming future.

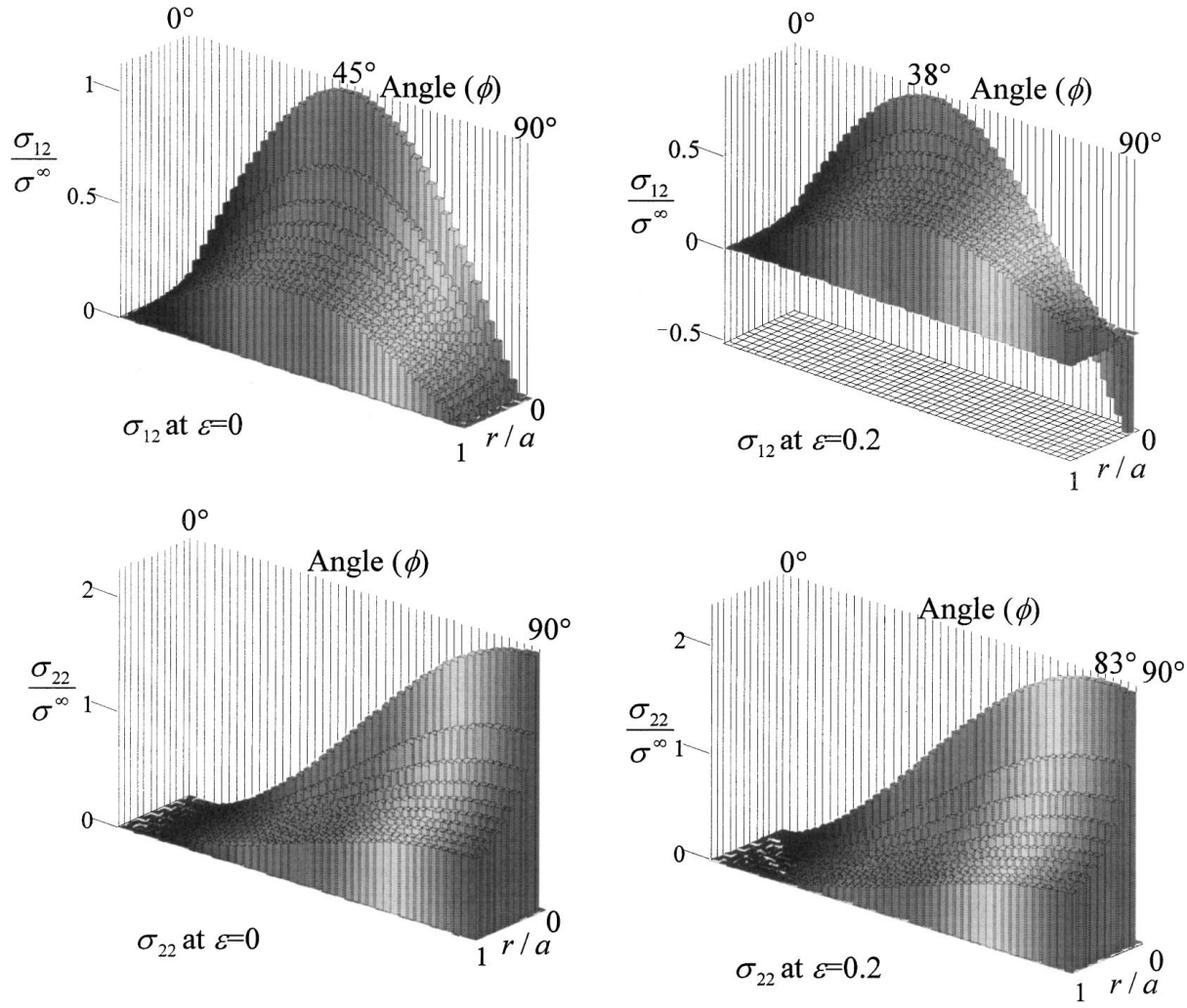

Figure 14 Normal (σ_{22}) and shear stress (σ_{12}) at the crack tip along interface of two dissimilar materials corresponding to angle (ϕ between directions of loading and interface), and distance (r) to the crack tip with respect to two different ε, i.e. 0 and 0.2.

5. Conclusions

Based on the experimental investigation, analyses of crystallography, and a model of interface mechanics, the following conclusions can be made:

(1) Concerning crack initiation, there are three noticeable characteristics, i.e. sudden crack initiating, site preference and orientation preference. For site preference, interface cracks prevail at the boundary of lamellae. In addition, there is small amount of "short" cracks at grain boundaries. The former gives a serious impact on the eventual failure. With regard to orientation preference, there are three notable peaks in orientations at $\psi = 40^\circ$, 60° and 90°.

(2) With respect to crack propagation, there are also three obvious characteristics, i.e. rapid propagating, translamellar-fracture-mode appearing and deflecting of propagating cracks. The two latter phenomena reflect the inclination for enhancing toughness owing to lamellar structure.

(3) Through studying in crystallography, we can deduce that adjacent lamellae of twins are prone to delaminating during either crack initiation or crack propagation due to its low NAT and geometric compatibility factor ($\tilde{m}$), and 120°-rotation pair with higher NAT and $\tilde{m}$ should be more resistant to crack initiating compared to 60°- or 180°-rotation pair of intervariant γ lamellae. As to the γ/α_2, it has the lowest $\tilde{m}$ but high NAT, thus, it may take different effects in respective crack initiation and crack propagation.

(4) A model of mechanics can semiquantitatively give a rough explanation for our experimental result about orientation peaks (ψ) of nucleated cracks, i.e. 40°, 60°, 90°. Cracking in 90°, 40° and 60° are mainly associated respectively with the normal stress (σ_{22}), the shear stress(σ_{12}) and a synergic impact from both σ_{12} and σ_{22}.

Acknowledgements

This paper was supported by the National Natural Science Foundation of China and the Chinese Academy of Sciences.

References

1. Y. W. KIM, in "Gamma Titanium Aluminides," edited by Y. W. Kim, R. Wagner and M. Yamaguchi (The Minerals, Metals & Materials Society, 1995) p. 637.
2. M. YAMAGUCHI and H. INUI, in "Structural Intermetallics," edited by R. Darolia, J. J. Lewandowski, C. T. Liu, P. L. Martin, D. B. Miracle and M. V. Nathal (The Minerals, Metals & Materials Society, 1993) p. 127.
3. M. A. MORRIS and M. LEBOEUF, *Materials Science and Engineering* **A224** (1997) 1.
4. D. M. DIMIDUK, *Mat. Res. Soc. Symp. Proc.* **364** (1995) 599.
5. S. ZGHAL, S. NAKA and A. COURET, *Acta Mater.* **45**(7) (1997) 3005.
6. M. FU, Y. HONG and L. ZHENG, in Fatigue'99, The Seventh International Fatigue Conference, edited by X. R. Wu and Z. G. Wang, 1999.
7. M. CHEN, D. CHEN and T. L. LIN, *Mat. Res. Soc. Symp. Proc.* **364** (1995) 1047.
8. J. LUSTER and M. A. MORRIS, *Metallurgical and Materials Transactions A* **26A** (7) (1995) 1754.
9. M. YAMAGUCHI, H. INUI, S. YOKOSHIMA, K. KISHIDA and D. R. JOHNSON, *Materials Science and Engineering* **A213** (1996) 25.
10. J. J. DUNDURS, *Journal of Applied Mechanics* **36** (1969) 650.
11. J. W. HUTCHINSON, M. E. MEAR and J. R. RICE, *ibid.* **54** (1987) 828.
12. J. R. RICE, *ibid.* **55** (1988) 98.
13. C. F. SHIH and R. J. ASARO, *ibid.* **55** (1988) 299.
14. T. L. BECKER JR., J. M. MCNANEY, R. M. CANNON and R. O. RITCHIE, *Mechanics of Materials* **25** (1997) 291.

Received 2 February 1999
and accepted 27 March 2000